

Physical Simulation of Moisture Induced Thin Shell Deformation

ANONYMOUS AUTHOR(S)

ACM Reference Format:

Anonymous Author(s). 2018. Physical Simulation of Moisture Induced Thin Shell Deformation. 1, 1 (November 2018), 8 pages. <https://doi.org/10.1145/888888.777777>

1 INTRODUCTION

Contribution. We present a low-order discrete shell model tailored to simulating non-uniform, anisotropic, differential swelling and shrinking of thin shells. In contrast to previous methods for simulating related phenomena, such as burning and growth, our formulation builds on discrete geometric shell theory and supports arbitrary rest curvature and strain, and physical settings such as thickness and Lamé parameters. We couple our shell model to a simple formulation of moisture diffusion in both the lateral and thickness directions, which takes into account anisotropy of the material grain. In a series of experiments, we show that our model successfully predicts the qualitative behavior of thin shells undergoing complex, dynamic deformations due to swelling or shrinking, such as occurs when paper is moistened, leaves dry in the sun, or thin plastic melts.

1.1 Related Work

Simulating Burning/Melting/Swelling. Several papers look at related problems, such as evolving the boundary of a burning or melting solid, without incorporating curling/wrinkling and other elastic deformations of the solid. Melek and Keyser [2003; 2005] simulate pyrolysis and heat diffusion of burning objects, but do not consider elastic deformation of the burning objects. Losasso et al [2006] proposed tracking of the burning boundary of thin shells using an adaptive level set on the shell. Some of the deformation can be qualitatively approximated by mapping physical quantities like heat and moisture to cells of a coarse grid around the object, deforming the cage, and mapping the deformation back onto the shell (as in Free Form Deformation); this approach was proposed by Melek and Keyser [2007] and adopted by Liu et al [2009]. Most similar to our work is the method of Jeong et al [2011; 2013], which uses a *bilayer* of springs (a triangle mesh and its circumcentric dual, offset a distance from the primal mesh) to represent the shell. The bilayer allows the method to capture *differential* growth due to gradients in moisture concentration across the thickness of leaves, leading to visually impressive simulations of leaves curling as they dry. Our work is based on the same fundamental idea (representing the shell using rest geometry that varies linearly through the thickness) but couched in the machinery of differential geometry; our formulation

Permission to make digital or hard copies of part or all of this work for personal or classroom use is granted without fee provided that copies are not made or distributed for profit or commercial advantage and that copies bear this notice and the full citation on the first page. Copyrights for third-party components of this work must be honored. For all other uses, contact the owner/author(s).

© 2018 Copyright held by the owner/author(s).
XXXX-XXXX/2018/11-ART
<https://doi.org/10.1145/888888.777777>

allows us to easily incorporate non-zero rest curvature, machine direction, and a physical material model.

Steps towards a principled physical model include the use of a mass-spring network to represent the shell, with update rules for how spring rest lengths should change due to physical processes in the shell. Such rules are simplest to formulate in the case where growth or shrinkage is uniform through the shell thickness, and the shell can be represented using a single spring layer; Larboulette et al [2013] present such a rule, which includes handling of the *machine direction* of paper: a bias in the orientation of the fibers composing the paper which causes the paper to swell anisotropically. We adopt this parameter in our material model.

Mechanics of Shells. The mathematics and geometry underpinning the physics of thin shells is a venerable topic: Ciarlet's book [2000] on elasticity as applied to shells offers a thorough overview. Our work is based on the common *Kirchhoff-Love* assumption that the shell does not undergo any transverse shear; ie, that the shell volume is foliated by normal offsets of the shell's *midsurface*: the problem of studying deformation of the 3D shell volume then reduces to that of deformation of a 2D surface, and tools from Riemannian geometry can be applied [Simo and Fox 1989]. (We adopt the so-called "intrinsic" view [Neff 2004] that shells can be understood in terms of Kirchhoff-Love and geometric principles, as this view allows us to easily discretize shell physics by leveraging discrete differential geometry, but we note in passing that the validity of the Kirchhoff-Love assumption, and of reduced shell models in general, remains unsettled, and the literature documents numerous alternative shell theories.) One key property of the shells we want to simulate is that they are *non-Euclidean*: they do not have a rest (strain-free) state that is realizable in three-dimensional space. Non-Euclidean shells have received substantial attention recently in the physics community [Kim et al. 2012; Klein et al. 2007], thanks to their potential applications in fabrication and robotics, and their connection to biological growth; Sharon and Efrati [Efrati et al. 2009; Sharon and Efrati 2010] pioneered the study of shell mechanics in this setting.

For the sake of being self-contained, we briefly review the geometric foundations of shell mechanics in Section 2.

Computational Modeling of Thin Shells. Thin shells first caught the interest of the graphics community in the context of simulating cloth [Baraff and Witkin 1998; Bridson et al. 2002]. These early methods tended to focus on thin *plates*, i.e. shells that are rest flat, and formulate shell dynamics either in terms of either hinge-based bending energies [Sullivan 2008; Tamstorf and Grinspun 2013] or the insight that the bending energy can be written in terms of the intrinsic Laplace-Beltrami operator applied to the shell's embedding function [Bergou et al. 2006; Bobenko and Schröder 2005; Wardetzky et al. 2007]. Grinspun et al [2003] introduced to graphics the simulation of shells with non-flat rest curvature. Their formulation is based on *differences of squared mean curvature*, leading to a simple

and easy-to-discrete bending energy; this model is physically suspect, however: consider a half-cylinder at rest when curled around the x -axis. Unbend the shell and re-bend it around the y -axis; the deformed configuration's strain cannot be captured by looking at mean curvature alone, as it is pointwise identical to the mean curvature of the rest configuration. Complete support for rest curvature requires a bending energy that incorporates full information about the extrinsic deformation of the shell [Grinspun et al. 2006]. One recent such discrete energy is described in Weischedel's under-appreciated work on discrete Cosserat shells [2012]; our exposition is modeled closely on hers, though we make different modeling choices (we use an intrinsic rather than Cosserat shell model, and require more flexible handling of the shell rest geometry).

Higher-order methods for simulating shells (including with e.g. NURBS or subdivision elements) are common in computational mechanics and isogeometric analysis [Bandara and Cirak 2018; Bathe et al. 1983; Batoz et al. 1980; Benson et al. 2010; Cirak et al. 2000; Kiendl et al. 2009] and have also been proposed for computer graphics [Wawrzinek et al. 2011]. High-order methods have some obvious advantages (better convergence behavior in the thin limit, especially for shell deformations involving large strains; continuous surface normals) at the cost of additional computational cost and complexity, especially when handling contact.

In this paper, we ignore the problem of mesh tesselation, or of adapting the mesh in response to either large deflections or large amounts of growth; such remeshing is an important component of a practical shell simulation but orthogonal to our focus on shell dynamics. ArcSim [Narain et al. 2012] incorporates a method of adaptive remeshing while avoiding significant popping artifacts, and has been used to generate impressive simulations of creasing paper. Vetter et al [2013] study the companion problem of remeshing due to large in-plane growth, and present a solution based on adaptive Loop subdivision.

2 CONTINUOUS FORMULATION

Before describing our discretization of shells, we briefly review the formulation in the continuous setting, as this formulation will guide our discretization.

Shell Geometry. We can represent shells $S \subset \mathbb{R}^3$ of thickness h by a parameter domain Ω in the plane and an embedding $\phi : \Omega \times [-h/2, h/2] \rightarrow \mathbb{R}^3$ with S the image of ϕ (see Figure ??). We adopt the common Kirchhoff-Love assumption that the shell does not undergo any transverse shear; ie, that the shell volume is foliated by normal offsets of the shell's *midsurface* $\mathbf{r} : \Omega \rightarrow \mathbb{R}^3$. In other words,

$$\phi(x, y, z) = \mathbf{r}(x, y) + z\hat{\mathbf{n}}(x, y)$$

where $\hat{\mathbf{n}} = (\mathbf{r}_x \times \mathbf{r}_y) / \|\mathbf{r}_x \times \mathbf{r}_y\|$ is the midsurface normal. The shell's deformation is thus completely determined by the deformation of the midsurface. The metric \mathbf{g} on the slab $\Omega \times [-h/2, h/2]$, pulled back from \mathbb{R}^3 , can be expressed in terms of the geometry of the midsurface:

$$\mathbf{g} = \begin{bmatrix} \mathbf{a} - 2z\mathbf{b} + z^2\mathbf{c} & 0 \\ 0 & 1 \end{bmatrix}, \quad (1)$$

where

$$\mathbf{a} = d\mathbf{r}^T d\mathbf{r} \quad \mathbf{b} = -d\mathbf{r}^T d\hat{\mathbf{n}} \quad \mathbf{c} = d\hat{\mathbf{n}}^T d\hat{\mathbf{n}}$$

are the classical first, second, and third fundamental forms of the surface \mathbf{r} .

Oftentimes, the parameterization domain of a thin shell is assumed to be also the rest state of the shell, so that the strain in the material of the shell can be determined directly from looking at \mathbf{g} . We cannot assume this: consider for instance a piece of paper whose center has been moistened by spilled coffee. The fibers in the coffee stain stretch; since they are confined by the surrounding non-wet region of the paper, the paper cannot globally stretch in such a way that both the wet and dry regions of the paper are simultaneously at rest. Instead, the paper will *buckle* out of plane, into a shape that compromises between relaxing the in-plane (stretching) strain and the introduced bending strain. At this point the paper's rest state is *non-Euclidean*—it is impossible to find any embedding of the paper into \mathbb{R}^3 that is entirely strain-free.

We therefore record the rest state of the shell using a *rest metric* $\bar{\mathbf{g}}(x, y, z)$.¹ Since our model is tailored to simulating differential in-plane swelling or shrinking across the thickness of the shell, we make the simplifying assumption that this rest metric is linear in the thickness direction, and does not affect the shell thickness:

$$\bar{\mathbf{g}}(x, y, z) = \bar{\mathbf{a}}(x, y) - 2z\bar{\mathbf{b}}(x, y).$$

A shell that begins a simulation at rest will simply have $\bar{\mathbf{a}} = \mathbf{a}$ and $\bar{\mathbf{b}} = \mathbf{b}$; similarly, in the case that the shell *does* have a rest state $\bar{\mathbf{r}}$ that is isometrically embeddable in \mathbb{R}^3 , \mathbf{a} and \mathbf{b} are the first and second fundamental forms of the surface $\bar{\mathbf{r}}$. Therefore \mathbf{a} and \mathbf{b} can be thought of as representing the “rest metric” and “rest curvature” of the shell, respectively.²

Finally, we cannot assume that the shell has uniform density, since different parts of the shell might gain or lose mass due to absorbing or releasing moisture. We therefore allow the density per unit *rest* volume $\rho(x, y)$ to vary over Ω . (In principle, we could also model the variation in density across the shell thickness; however doing so leads only to a small ($O(h^3)$) correction to the shell's kinetic energy, and since the swelling phenomena we are interested in simulating tend to happen over relatively long time scales, there is no need for such accuracy.)

To summarize, our parameterization of thin shells involves the following kinematic elements:

- a thickness h and parameterization domain $\Omega \subset \mathbb{R}^2$, both of which are fixed over the course of the simulation;
- an embedding $\mathbf{r} : \Omega \rightarrow \mathbb{R}^3$ representing the shell midsurface's “current”/“deformed” geometry, and which evolves over time. From this midsurface embedding, the embedding of the full shell volume ϕ , and the midsurface fundamental forms, can be calculated;
- a rest metric and density, parameterized by the pair of tensor field $\bar{\mathbf{a}}, \bar{\mathbf{b}}$ and a scalar field ρ over Ω , respectively. These might also evolve over time, due to changes in the shell rest state via growth or shrinkage.

¹Here and throughout the paper, we use an overbar to denote quantities associated to the shell rest state.

²We stress, though, that these labels are to provide intuition only— $\bar{\mathbf{a}}$ and $\bar{\mathbf{b}}$ must not, and generally will not, satisfy usual relationships from differential geometry such as the Gauss-Codazzi-Mainardi equations.

2.1 Shell Dynamics

Motivated by the common observation that a sufficiently thin shell bends much more readily than it will stretch, we assume that the shell's deformation involves *large rotations* but only small in-plane strain of the midsurface: $\|\bar{\mathbf{a}}^{-1}\mathbf{a} - \mathbf{I}\|_\infty < h$. We also assume that the shell's material is uniform and isotropic. The simplest constitutive law consistent with these assumptions is to use a St. Venant-Kirchhoff material model³ together with Green strain; it can be shown [?] that these choices yield an elastic energy density (the *Koiter shell model*) that can be approximated up to $O(h^4)$ by

$$W(x, y) = \left(\frac{h}{4} \|\bar{\mathbf{a}}^{-1}\mathbf{a} - \mathbf{I}\|_{SV}^2 + \frac{h^3}{12} \|\bar{\mathbf{a}}^{-1}(\mathbf{b} - \bar{\mathbf{b}})\|_{SV}^2 \right) \sqrt{\det \bar{\mathbf{a}}} \quad (2)$$

where $\|\cdot\|_{SV}$ is the "St. Venant-Kirchhoff norm" [Weischedel 2012]

$$\|M\|_{SV} = \frac{\alpha}{2} \operatorname{tr}^2 M + \beta \operatorname{tr}(M^2),$$

for Lamé parameters α, β . In terms of the Young's modulus E and Poisson's ratio ν ,

$$\alpha = \frac{Ev}{(1+\nu)(1-2\nu)}, \quad \beta = \frac{E}{2(1+\nu)}.$$

We thus have a formulation of kinetic energy and potential energy

$$T[\mathbf{f}] = \int_{\Omega} h\rho \|\dot{\mathbf{r}}\|^2 \sqrt{\det \bar{\mathbf{a}}} dx dy, \quad V[\mathbf{r}] = \int_{\Omega} W(x, y) dx dy,$$

to which additional external energies and forces (gravity, constraint forces, etc) can be added to yield equations of motion via the usual principle of least action.

3 DISCRETIZATION

We approximate the midsurface \mathbf{r} with a triangle mesh (V, E, F) ; the positions of the vertices $\mathbf{v} = [\mathbf{v}_1, \mathbf{v}_2 \dots]$ take the place of the embedding function \mathbf{r} . The general strategy we will use is to assume that \mathbf{a} and \mathbf{b} , as well as their rest counterparts $\bar{\mathbf{a}}$ and $\bar{\mathbf{b}}$, are constant over each face of a triangle mesh representing the shell midsurface; it will then be relatively straightforward to write down a discrete analogue of the Koiter elastic energy density in Equation (2).

Discrete Shell Model. As in the continuous setting, the discrete shell does not necessarily have a rest state embeddable as a mesh in \mathbb{R}^3 , making it impossible to parameterize the deformed configuration of the shell in terms of the rest configuration; additionally we do not want to assume (or compute) a global parameterization of the midsurface. Instead, we independently parameterize each triangle in its own barycentric coordinates (see Figure ??). Let \mathbf{f}_{ijk} be a face in F containing the vertices $\mathbf{v}_i, \mathbf{v}_j, \mathbf{v}_k$, and denote by \mathcal{T} the canonical unit triangle with vertices $(0, 0), (1, 0), (0, 1)$. Then locally the face \mathbf{f}_{ijk} is embedded by the affine function

$$\mathbf{r}_{ijk} : \mathcal{T} \rightarrow \mathbb{R}^3, \quad \mathbf{r}_{ijk}(u_1, u_2) = \mathbf{v}_i + u_1(\mathbf{v}_j - \mathbf{v}_i) + u_2(\mathbf{v}_k - \mathbf{v}_i);$$

under this embedding, the Euclidean metric on face \mathbf{f}_{ijk} pulls back to the constant first fundamental form

$$\mathbf{a}_{ijk} = \begin{bmatrix} \|\mathbf{v}_j - \mathbf{v}_i\|^2 & (\mathbf{v}_j - \mathbf{v}_i) \cdot (\mathbf{v}_k - \mathbf{v}_i) \\ (\mathbf{v}_j - \mathbf{v}_i) \cdot (\mathbf{v}_k - \mathbf{v}_i) & \|\mathbf{v}_k - \mathbf{v}_i\|^2 \end{bmatrix}$$

³The neo-Hookean material model is also popular in computer graphics and could be used instead, although there is little benefit to doing so when simulating thin shells since strains are typically small.

on \mathcal{T} . If we are given an explicit rest configuration $\bar{\mathbf{v}}_i$ of the shell, we can compute the rest first fundamental form $\bar{\mathbf{a}}_{ijk}$ analogously; or alternatively we can set $\bar{\mathbf{a}}_{ijk}$ to any desired symmetric positive-definite 2×2 matrix. Notice that any such matrix corresponds to some choice of "rest lengths" for the edges of face \mathbf{f}_{ijk} that obey the triangle inequality, but that two faces sharing a common edge do not necessarily agree about that length.

These discrete fundamental forms are enough to discretize the stretching term in Equation (2): each face contributes a term

$$\begin{aligned} & \int_{\mathcal{T}} \frac{h}{4} \|\bar{\mathbf{a}}_{ijk}^{-1} \mathbf{a}_{ijk} - \mathbf{I}\|_{SV}^2 \sqrt{\det \bar{\mathbf{a}}_{ijk}} \\ &= \frac{h}{8} \|\bar{\mathbf{a}}_{ijk}^{-1} \mathbf{a}_{ijk} - \mathbf{I}\|_{SV}^2 \sqrt{\det \bar{\mathbf{a}}_{ijk}}. \end{aligned}$$

This energy is quartic in the positions of the mesh vertices, and is exactly the energy of constant-strain triangle stretching elements commonly used in cloth simulation.

For the bending term, we also need a discretization of the second fundamental form. Here there is a significant departure between the smooth theory and the discrete approximation: we would like to apply the Kirchhoff-Love principle to extrude the mid-surface into a shell volume, but unfortunately distance offsets of triangle meshes are no longer guaranteed to be triangle meshes (or even piecewise-affine). One can instead look at weaker notions of mesh parallelity [Bobenko et al. 2010]:

- *vertex offsets* require choosing a normal at each mesh vertex (itself a problem without an obvious solution), and moving each vertex a constant distance along this normal usually does not result in faces parallel to the original faces;
- *edge offsets* likewise do not guarantee parallel faces;
- *face offsets* are not conforming: moving each face around a vertex of valence four or higher in their normal direction yields new faces that are not guaranteed to still intersect at a common point.

We use the discretization that arises from edge parallelity, leading to the so-called "mid-edge" discretization of the second fundamental form [Grinspun et al. 2006; Weischedel 2012]: let \mathbf{e}_i denote the edge opposite vertex i on face \mathbf{f}_{ijk} , and define the *mid-edge normal* $\hat{\mathbf{n}}_i$ by:

- the face normal $\frac{(\mathbf{v}_j - \mathbf{v}_i) \times (\mathbf{v}_k - \mathbf{v}_i)}{\|(\mathbf{v}_j - \mathbf{v}_i) \times (\mathbf{v}_k - \mathbf{v}_i)\|}$, if \mathbf{e}_i is a boundary edge;
- the mean of the face normals of the two faces incident on \mathbf{e}_i , otherwise.

Let $\mathbf{f}_{ijk}^\epsilon$ denote the triangle formed by offsetting all of \mathbf{f}_{ijk} 's edges in their mid-edge normal direction by a distance ϵ , and let $\mathbf{a}_{ijk}^\epsilon$ be the discrete first fundamental form of that offset triangle. Then the discrete second fundamental form \mathbf{b} can be defined, by analogy to Equation (1), as the first-order correction

$$\mathbf{a}_{ijk}^\epsilon = \mathbf{a}_{ijk} - 2\epsilon \mathbf{b}_{ijk} + O(\epsilon^2),$$

leading to the formula

$$\mathbf{b}_{ijk} = \frac{1}{2} \begin{bmatrix} (\hat{\mathbf{n}}_i - \hat{\mathbf{n}}_j) \cdot (\mathbf{v}_i - \mathbf{v}_j) & (\hat{\mathbf{n}}_i - \hat{\mathbf{n}}_j) \cdot (\mathbf{v}_i - \mathbf{v}_k) \\ (\hat{\mathbf{n}}_i - \hat{\mathbf{n}}_k) \cdot (\mathbf{v}_i - \mathbf{v}_j) & (\hat{\mathbf{n}}_i - \hat{\mathbf{n}}_k) \cdot (\mathbf{v}_i - \mathbf{v}_k) \end{bmatrix}.$$

(Alternatively, this formula can be derived by discretizing the relation $\mathbf{b} = -d\mathbf{r}^T d\hat{\mathbf{n}}$ using divided differences). Although it may not appear so at first, the matrix \mathbf{b}_{ijk} is always symmetric (since each

mid-edge normal is orthogonal to that edge); it is not in general positive-definite.⁴ We represent the rest second fundamental form \bar{b}_{ijk} by an arbitrary symmetric 2×2 matrix assigned to each face.

Choosing Rest Fundamental Forms. Depending on the mechanism for growth being simulated, there are several choices for how to set and update \bar{a} and \bar{b} :

- **No Growth:** A classic shell, whose rest state is fixed, simply has $\bar{a} = a^0$ and $\bar{b} = b^0$, where a^0 denotes the first fundamental form induced by v^0 , the positions of the midsurface vertices at the beginning of the simulation. (And if the shell is pre-stressed, \bar{a}, \bar{b} can be adjusted appropriately).

- **Isotropic Growth:** In many cases growth is isotropic and uniform through the thickness of the shell (for instance, when plastic shrinks in response to heat, or plant tissue grows through cell division). In this case

$$\bar{a} = e^{2s_{ijk}} a^0, \quad \bar{b} = b^0$$

for a conformal factor s encoding the amount of growth (or shrinking, if negative).

- **Differential Swelling:** Porous materials like paper swell when moistened, and differences in water concentration through the thickness of a thin shell can induce metric frustration and buckling. This mechanism is responsible for the buckling of paper when wet, and the curling of leaves as they dry. We assume that the amount of moisture varies linearly in the thickness direction of the shell, and represent the saturation of the shell on each face by two scalars $m_{ijk}^+, m_{ijk}^- \in [0, 1]$, so that the saturation at distance z from the mid-surface is given by $\frac{(2z+h)m_{ijk}^- + (2z-h)m_{ijk}^+}{2h}$. The water saturation induces swelling, which changes the rest geometry,

Elastic Energy. We can now write down the full elastic energy of the shell, in exact analogy to the Koiter energy:

$$E_{\text{elastic}}(v) = \sum_{f_{ijk} \in F} \frac{\sqrt{\det \bar{a}_{ijk}}}{2} \left(\frac{h}{4} \|\bar{a}_{ijk}^{-1} a_{ijk} - I\|_{SV}^2 + \frac{h^3}{12} \|\bar{a}_{ijk}^{-1} (b_{ijk} - \bar{b}_{ijk})\|_{SV}^2 \right)$$

It is worth making a few observations about this energy. First, the matrices a, \bar{a} , etc. are *coordinate-dependent*: replacing the parameterization domain \mathcal{T} , or even cyclically permuting the order of vertices around a face, would alter the values in the matrix. However, the generalized eigenvalues of $a - \bar{a}$ and $b - \bar{b}$ with respect to the inner product \bar{a} are *coordinate-independent*, as is the total energy. Perhaps the easiest way to see this fact is to note that these spectra measure the geometrically exact strain induced by an affine embedding of \mathcal{T} , and so *must* be independent of the coordinates chosen. Second, the terms of the form $\|\bar{a}^{-1} M\|_{SV}^2$ are sometimes instead written

⁴As observed by Grinspun et al [2006], the *shape operator* $d\hat{n}$ in the continuous setting always maps tangent vectors to tangent vectors, whereas in the discrete setting the finite difference of mid-edge normals is not always parallel to the mesh triangle. This discrepancy is a consequence of the failure of edge-offset meshes to also be face-offsets. Corrections to the shape operator have been proposed to remedy this quirk, though we found them unnecessary (and in any case, any components of $d\hat{n}$ that lie orthogonal to the face are annihilated when forming the second fundamental form $-dr^T d\hat{n}$).

as $\|\bar{a}^{-1/2} M \bar{a}^{-1/2}\|_{SV}^2$, where $\bar{a}^{-1/2}$ is the unique positive-definite square root of \bar{a} . The two expressions are equivalent, since the spectrum of a product of matrices is invariant under cyclic permutation, but the form used above is slightly more convenient for computation. Finally, as a sanity check, observe that when $\bar{b} = 0$ and the Poisson ratio $\nu = 0$, the bending energy reduces to the square of mean curvature, as expected for thin plates.

Mass Matrix. As in the continuous formulation, the density ρ_{ijk} of each face might change over time due to absorption or evaporation of moisture. We use a piecewise-constant discretization of density

$$\rho_{ijk} = \rho_{\text{shell}} + \frac{m_{ijk}^+ + m_{ijk}^-}{2} \rho_{\text{water}},$$

where ρ_{shell} and ρ_{water} are the densities of the shell material and water, respectively, and construct a typical Galerkin mass matrix M for the midsurface vertices. (In simulations where shell deformation is driven by a mechanism other than moisture changes, we drop the second term and use a constant density.)

Viscous Damping. Since the growth and swelling phenomena we want to simulate all take place at relatively long time scales, and paper and plastic are viscoelastic, a damping model is needed to dissipate the elastic waves in the material. We implement a simple Kelvin-Voigt damping model by including a damping potential

$$E_{\text{damp}}(v, v^{\text{prev}}) = \eta \Delta t \sum_{f_{ijk} \in F} \frac{\sqrt{\det \bar{a}_{ijk}}}{2} \left(\frac{h}{4} \left\| \bar{a}_{ijk}^{-1} \frac{a_{ijk} - a_{ijk}^{\text{prev}}}{\Delta t} \right\|_{SV}^2 + \frac{h^3}{12} \left\| \bar{a}_{ijk}^{-1} \frac{b_{ijk} - b_{ijk}^{\text{prev}}}{\Delta t} \right\|_{SV}^2 \right)$$

where Δt is the time step size, v^{prev} denotes the values of v in the previous time step (and likewise for a^{prev} , etc), and η is a viscosity parameter.

Summary. In the discrete simulation, we track the following variables:

- The configuration v and configurational velocity \dot{v} . These vertex positions completely encode the kinematics of the discrete shell.
- Two matrices \bar{a} and \bar{b} per face in F , both symmetric, and with \bar{a} positive-definite. These matrices store information about the rest state of the discrete shell, and may change over the course of the simulation. In most of our simulations, the mechanism for changes in the shell rest state is absorption or evaporation of moisture; in this case we store two scalars m^+ and m^- per face, indicating moisture concentration on the top and bottom boundary of the shell, and \bar{a} and \bar{b} are computed from these scalars, as described above.

In addition, we track a machine direction d per face, which doesn't change over the course of the simulation; finally Table ?? lists the physical parameters and constants on which the simulation depends, as well as reasonable values of these parameters for the special case of ordinary paper. We use these default values in all experiments described below, unless specified otherwise.

457 *Time Integration.* We integrate the equations of motion using
 458 implicit Euler:

$$459 \quad M \frac{\dot{\mathbf{v}}^{i+1} - \dot{\mathbf{v}}^i}{\Delta t} = \mathbf{F}_{\text{ext}}(\mathbf{v}^{i+1}) - \nabla E_{\text{elastic}}(\mathbf{v}^{i+1}) - \nabla E_{\text{damp}}(\mathbf{v}^{i+1}, \mathbf{v}^i) \\ 460 \quad \mathbf{v}^{i+1} = \mathbf{v}^i + \Delta t \dot{\mathbf{v}}^{i+1},$$

463 where superscripts denote the time step index and \mathbf{F}_{ext} encapsulates contact forces and external forces like gravity. Solving these
 464 equations requires computing first and second derivatives of the
 465 elastic energy; the derivatives of a triangle's stretching term depend
 466 only on the vertices of that triangle, whereas the derivatives of the
 467 bending term also depend on vertices of the neighboring three tri-
 468 angles (due to the dependence of \mathbf{b} on the mid-edge normals). The
 469 bending term in particular is somewhat unpleasant to differentiate
 470 due to its high degree of nonlinearity, and special cases that arise
 471 for triangles adjacent to the mesh boundary. We provide formulas
 472 for the derivatives in the Appendix, and source code for calculating
 473 the derivatives in the supplemental material.

4 MOISTURE DIFFUSION

5 RESULT

479 We evaluate the simulation on a variety of examples, both didactic
 480 and complex.

5.1 Analytic Benchmarks

483 We first test the method on examples where the equilibrium state
 484 can be computed exactly. When an embedding \mathbf{r} exists for which
 485 $\mathbf{a} = \bar{\mathbf{a}}$ and $\mathbf{b} = \bar{\mathbf{b}}$, that embedding is clearly a global minimizer of
 486 the elastic energy, regardless of material parameters. We ran all of
 487 the following experiments using the default values in Table ???. We
 488 assigned a viscosity $\gamma = XXX$ to the material and ran the simulation
 489 for YYY seconds, enough time for the simulation to reach steady
 490 state.

492 *Uniform Swelling of Square.* We take Ω to be a unit square, with
 493 $\mathbf{r} = \text{id}$, and assign a constant $\bar{\mathbf{a}}$ and $\bar{\mathbf{b}}$ to the entire shell. Table 1
 494 summarizes the values of $\bar{\mathbf{a}}$ and $\bar{\mathbf{b}}$ we tried, and the expected shape
 495 and curvatures of the exact solution. We ran the simulation using
 496 a coarse, fine, and nonuniform mesh (XXX, YYY, and ZZZ vertices
 497 respectively); simulated and exact solutions are compared in Figure ???. For all experiments except the hyperboloid, we compute the
 498 Hausdorff error between the steady state simulation mesh and the
 499 analytic solution. The hyperboloid does not have a single equilib-
 500 rium state; the energy landscape is "sombrero-like" with a curve of
 501 possible solutions, corresponding to intrinsic rotation of the hyper-
 502 boloid. For this experiment we instead measure the sum of squared
 503 mean and Gauss curvature, where the mesh's curvatures were mea-
 504 sured using quadratic fitting [?].

507 *Isotropic Growth.* The Riemann mapping theorem guarantees that
 508 every surface M with disk topology can be parameterized by the unit
 509 disk, with metric conformally equivalent to the Euclidean metric.
 510 This insight was exploited by Kim et al [] to grow a sphere from a
 511 square. In the case that M is flat, and this conformal metric is $\mathbf{a} = e^{2s} I$
 512 for conformal factor s , then a disk with prescribed fundamental

49 forms

$$514 \quad \bar{\mathbf{a}} = e^{2s} I, \quad \bar{\mathbf{b}} = 0$$

515 is expected to grow into M (up to rigid motion), since M is a global
 516 minimizer of the elastic energy. We use this fact as a basis for a test:
 517 we conformally map a XXX to the unit disk using the method of
 518 Crane [], assign a rest metric $\bar{\mathbf{a}}$ per the above formula, and simulate
 519 the resulting growth of the shell. Figure ?? compares the initial shape
 520 to the simulation steady state.

521 When M is not flat, we do not expect the shell to grow exactly into
 522 the shape M , since embedding the shell as the shape M minimizes
 523 stretching energy while ignoring bending energy. Nevertheless, we
 524 expect the steady state geometry to closely resemble M , especially
 525 for small shell thickness h . Figure ?? shows the result of attempting
 526 to swell the unit disk into a sphere, using the rest fundamental forms
 527 from Kim et al [?],

$$528 \quad \bar{\mathbf{a}} = XXX, \quad \bar{\mathbf{b}} = 0.$$

5.2 Comparisons to Experiments

Radial Swelling of Disk.

Curling of Paper.

5.3 Effects of Parameters

Poisson's Ratio.

Thickness.

Machine Direction.

5.4 Comparison to Jeong et al

5.5 Qualitative Experiments

We end with several experiments that demonstrate the flexibility
 545 of the method to simulate complex geometry undergoing complex
 546 nonlinear deformations due to differential swelling.

The Walker.

The Caterpillar.

The Spoon.

6 OLD TEXT

6.0.1 Radially Wet Disc.

6.0.2 Machine Direction Experiment.

6.0.3 Dried Leaves.

6.0.4 Wetting Paper Annulus.

6.0.5 Wetting Straw Wrapping Paper.

6.0.6 Melting Spoon.

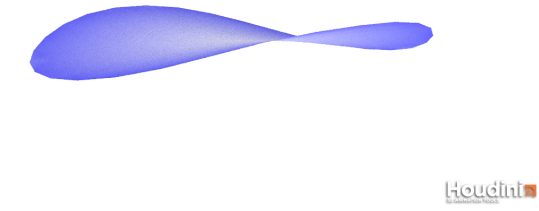
6.0.7 Melting Torus.

7 CONCLUSIONS AND FUTURE WORK

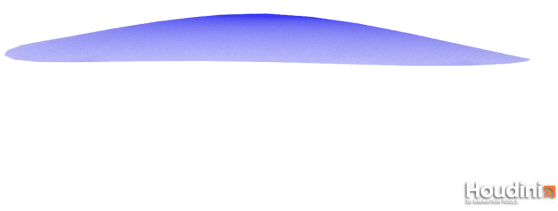
REFERENCES

Kosala Bandara and Fehmi Cirak. 2018. Isogeometric shape optimisation of shell structures using multiresolution subdivision surfaces. *Computer-Aided Design* 95, Supplement C (2018), 62 – 71. <https://doi.org/10.1016/j.cad.2017.09.006>

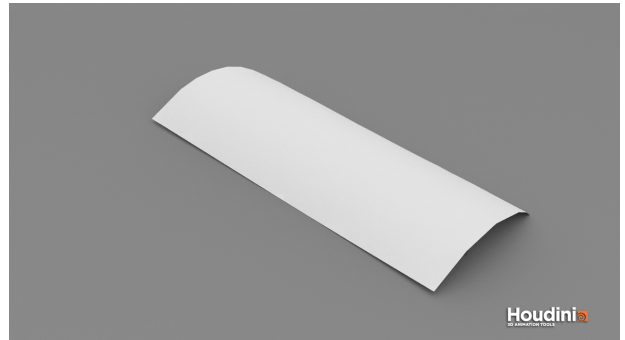
Table 1. Didactic experiments on a unit square. Different \bar{a} and \bar{b} are prescribed uniformly over the square, and in each case we compare the simulated steady state to the expected analytic solution.



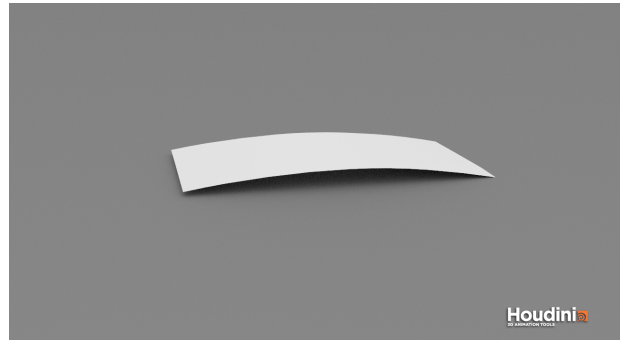
(a) Caption1



(b) Caption 2



(a) Caption1



(b) Caption 2

- David Baraff and Andrew Witkin. 1998. Large Steps in Cloth Simulation. In *Proceedings of the 25th Annual Conference on Computer Graphics and Interactive Techniques (SIGGRAPH '98)*. ACM, New York, NY, USA, 43–54. <https://doi.org/10.1145/280814.280821>

Klaus JÃ¼rgen Bathe, Eduardo Dvorkin, and Lee W. Ho. 1983. Our discrete-Kirchhoff and isoparametric shell elements for nonlinear analysisâ†An assessment. *Computers & Structures* 16, 1 (1983), 89 – 98. [https://doi.org/10.1016/0045-7949\(83\)90150-5](https://doi.org/10.1016/0045-7949(83)90150-5)

Jean-Louis Batoz, Klaus JÃ¼rgen Bathe, and Lee-Wing Ho. 1980. A study of three-node triangular plate bending elements. *Internat. J. Numer. Methods Engrg.* 15, 12 (1980), 1771–1812. <https://doi.org/10.1002/nme.1620151205>

D.J. Benson, Y. Bazilevs, M.C. Hsu, and T.J.R. Hughes. 2010. Isogeometric shell analysis: The ReissnerâŠMindlin shell. *Computer Methods in Applied Mechanics and Engineering* 199, 5 (2010), 276 – 289. <https://doi.org/10.1016/j.cma.2009.05.011> Computational Geometry and Analysis.

Miklos Bergou, Max Wardetzky, David Harmon, Denis Zorin, and Eitan Grinspun. 2006. A Quadratic Bending Model for Inextensible Surfaces. In *Proceedings of the Fourth Eurographics Symposium on Geometry Processing (SGP '06)*. Eurographics

, Vol. 1, No. 1, Article . Publication date: November 2018.

2017-11-30 12:49 page 6 (pp. 1-8)

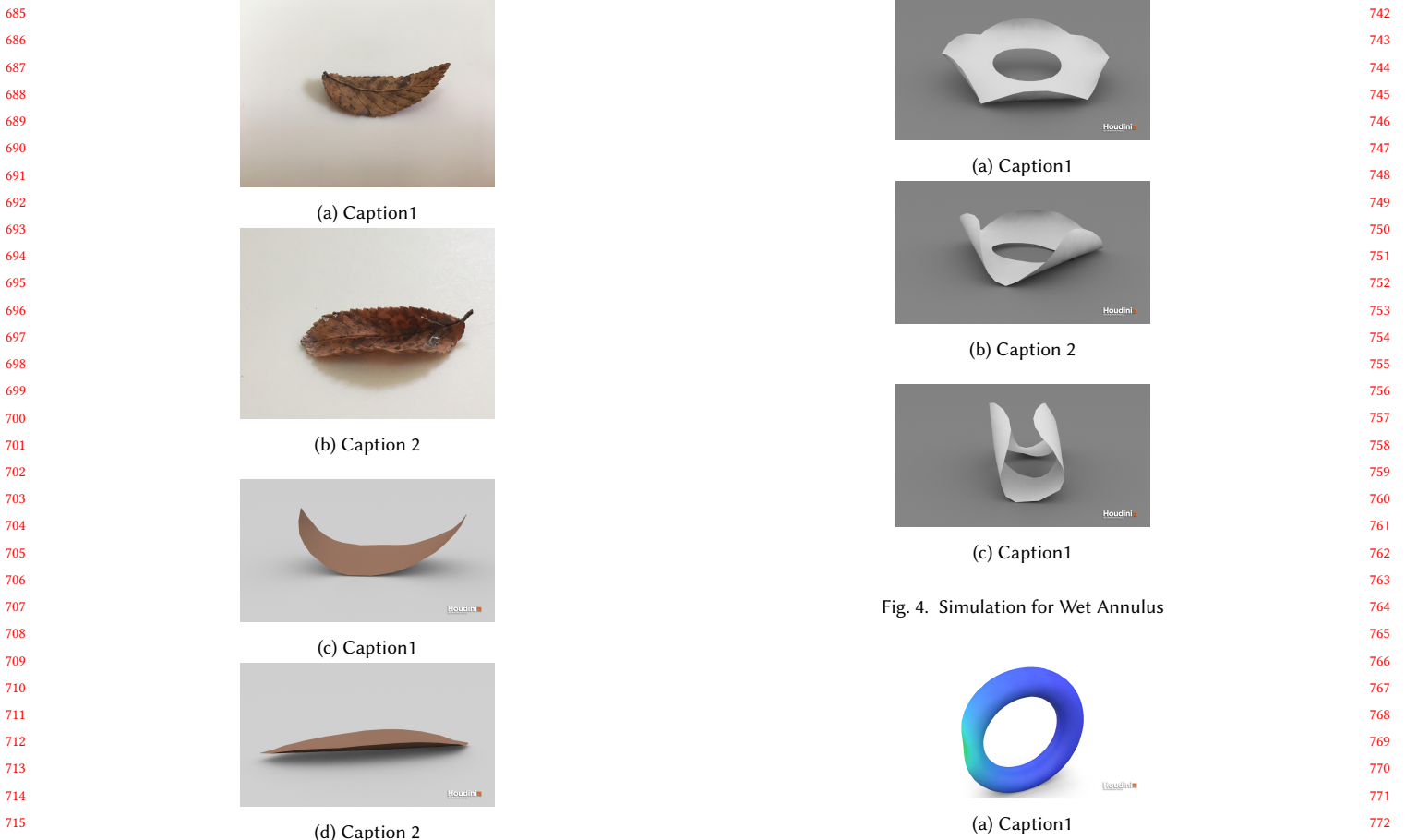


Fig. 3. Simulation for Dried Leaves

Fig. 4. Simulation for Wet Annulus

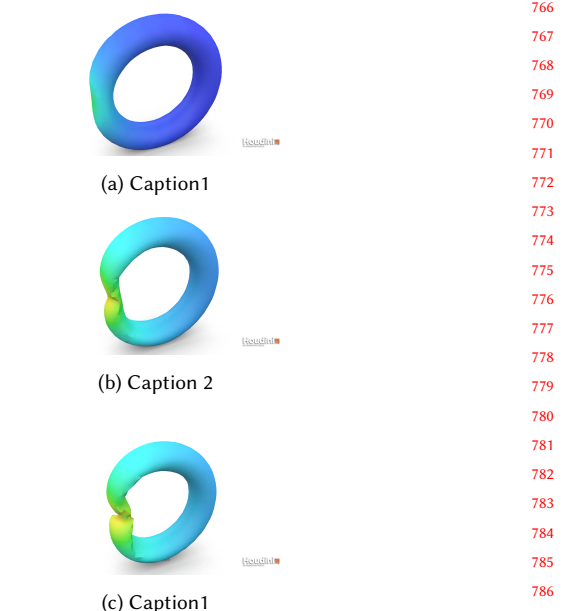


Fig. 5. Simulation for Dried Torus

- Frank Losasso, Geoffrey Irving, Eran Guendelman, and Ron Fedkiw. 2006. Melting and Burning Solids into Liquids and Gases. *IEEE Transactions on Visualization and Computer Graphics* 12, 3 (May 2006), 343–352. <https://doi.org/10.1109/TVCG.2006.51>
- Zeki Melek and John Keyser. 2003. Interactive Simulation of Burning Objects. In *Proceedings of the 11th Pacific Conference on Computer Graphics and Applications (PG '03)*. IEEE Computer Society, Washington, DC, USA, 462–. <http://dl.acm.org/citation.cfm?id=946250.946923>
- Zeki Melek and John Keyser. 2005. Multi-representation Interaction for Physically Based Modeling. In *Proceedings of the 2005 ACM Symposium on Solid and Physical*

799	Modeling (SPM '05). ACM, New York, NY, USA, 187–196. https://doi.org/10.1145/1060244.1060265	856
800	Zeki Melek and John Keyser. 2007. Driving Object Deformations from Internal Physical Processes. In <i>Proceedings of the 2007 ACM Symposium on Solid and Physical Modeling (SPM '07)</i> . ACM, New York, NY, USA, 51–59. https://doi.org/10.1145/1236246.1236257	857
801	Rahul Narain, Armin Samii, and James F. O'Brien. 2012. Adaptive Anisotropic Remeshing for Cloth Simulation. <i>ACM Trans. Graph.</i> 31, 6, Article 152 (Nov. 2012), 10 pages. https://doi.org/10.1145/2366145.2366171	858
802	P. Neff. 2004. A geometrically exact Cosserat shell-model including size effects, avoiding degeneracy in the thin shell limit. Part I: Formal dimensional reduction for elastic plates and existence of minimizers for positive Cosserat couple modulus. <i>Continuum Mechanics and Thermodynamics</i> 16, 6 (01 Oct 2004), 577–628. https://doi.org/10.1007/s00161-004-0182-4	859
803	Eran Sharon and Efi Efrati. 2010. The mechanics of non-Euclidean plates. <i>Soft Matter</i> 6 (2010), 5693–5704. Issue 22. https://doi.org/10.1039/C0SM00479K	860
804	J.C. Simo and D.D. Fox. 1989. On a stress resultant geometrically exact shell model. Part I: Formulation and optimal parametrization. <i>Computer Methods in Applied Mechanics and Engineering</i> 72, 3 (1989), 267 – 304. https://doi.org/10.1016/0045-7825(89)90002-9	861
805	John M. Sullivan. 2008. <i>Curvatures of Smooth and Discrete Surfaces</i> . Birkhäuser Basel, Basel, 175–188. https://doi.org/10.1007/978-3-7643-8621-4_9	862
806	Rasmus Tamstorf and Eitan Grinspun. 2013. Discrete bending forces and their Jacobians. <i>Graphical Models</i> 75, 6 (2013), 362 – 370. https://doi.org/10.1016/j.gmod.2013.07.001	863
807	Roman Vetter, Norbert Stoop, Thomas Jenni, Falk K. Wittel, and Hans-Jürgen Härmann. 2013. Subdivision shell elements with anisotropic growth. <i>Internat. J. Numer. Methods Engrg.</i> 95, 9 (2013), 791–810. https://doi.org/10.1002/nme.4536	864
808	Max Wardetzky, Miklós Bergou, David Harmon, Denis Zorin, and Eitan Grinspun. 2007. Discrete Quadratic Curvature Energies. <i>Comput. Aided Geom. Des.</i> 24, 8-9 (Nov. 2007), 499–518. https://doi.org/10.1016/j.cagd.2007.07.006	865
809	Anna Wawrzinek, Klaus Hildebrandt, and Konrad Polthier. 2011. Koiter's Thin Shells on Catmull-Clark Limit Surfaces. In <i>Vision, Modeling, and Visualization (2011)</i> , Peter Eisert, Joachim Hornegger, and Konrad Polthier (Eds.). The Eurographics Association. https://doi.org/10.2312/PE/VMV/VMV11/113-120	866
810	Claris Weischedel. 2012. <i>A discrete geometric view on shear-deformable shell models</i> . Ph.D. Dissertation. Georg-August-Universität Göttingen.	867
811		868
812		869
813		870
814		871
815		872
816		873
817		874
818		875
819		876
820		877
821		878
822		879
823		880
824		881
825		882
826		883
827		884
828		885
829		886
830		887
831		888
832		889
833		890
834		891
835		892
836		893
837		894
838		895
839		896
840		897
841		898
842		899
843		900
844		901
845		902
846		903
847		904
848		905
849		906
850		907
851		908
852		909
853		910
854		911
855		912